

NMR study of ion dynamics and charge storage in ionic liquid supercapacitors

Supporting Information

Alexander C. Forse,^a John M. Griffin,^a Céline Merlet,^a Paul M. Bayley,^a Hao Wang,^a Patrice Simon,^{c,d} Clare P. Grey^{*a,b}

^aDepartment of Chemistry, University of Cambridge, Lensfield Road, Cambridge CB2 1EW, U.K.

^bDepartment of Chemistry, Stony Brook University, Stony Brook, New York 11794-3400, United States

^cUniversité Paul Sabatier Toulouse III, CIRIMAT, UMR-CNRS 5085, F-31062 Toulouse, France

^dRéseau sur le Stockage Electrochimique de l'Energie (RS2E), FR CNRS n°34059, France

S1. Static spectra of charged electrodes

S2. Time dependence of spectra for electrodes from disassembled coin cells

S3. Spectral deconvolutions of *ex situ* NMR data

S4. Variation of anisotropy upon charging

S5. Variation of ¹⁹F chemical shift for TFSI anions as a function of temperature

S6. Variable temperature ¹H NMR spectra of YP50F soaked with ionic liquid

S7. Multisite model for exchange

S8. Spectra for YP50F soaked with EMITFSI/dACN

S1. Static spectra of charged electrodes

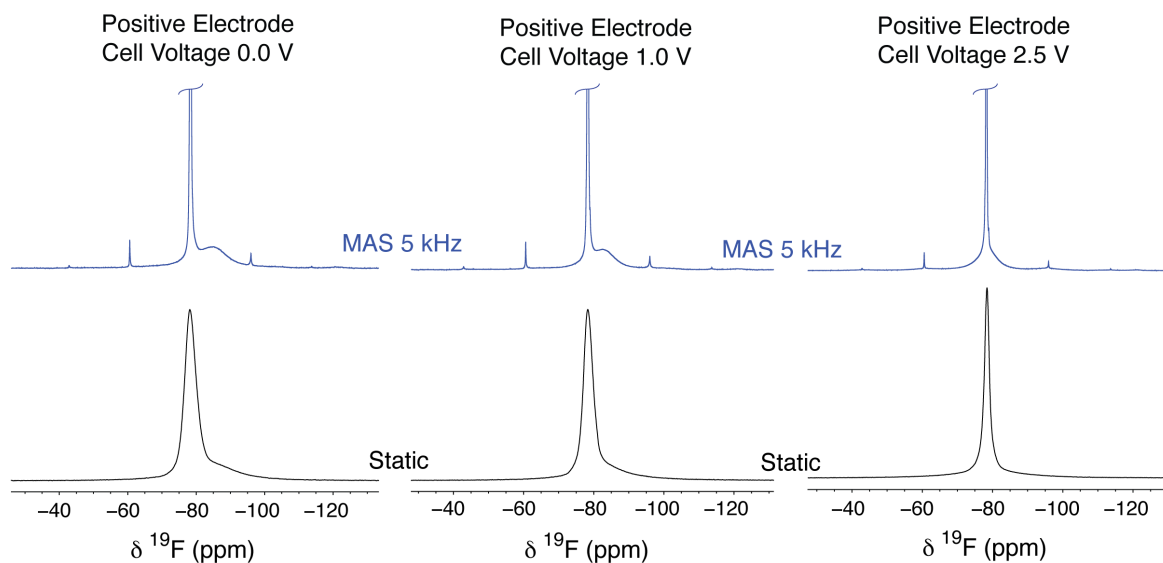


Figure S1 ^{19}F NMR spectra recorded at 7.1 T, for positive electrodes extracted from disassembled coin cell supercapacitors with different states of charge. Static and MAS 5 kHz spectra are shown for each sample.

^{19}F NMR spectra were recorded on static samples extracted from charged coin cells to explore the resolution that could be achieved (Figure S1). While it is possible to observe a broad in-pore shoulder in the 0 V spectrum, it is not well resolved. As the cell voltage is increased and the in-pore resonance shifts to higher frequency, the resolution becomes increasingly poor. At a cell voltage of 2.5 V it is very difficult to make out the in-pore resonance. MAS spectra (at 5 kHz) of the same samples are also shown in Figure S1. These spectra show much better resolution of the in-pore resonance over the range of voltages studied.

S2. Time dependence of spectra for electrodes from disassembled coin cells

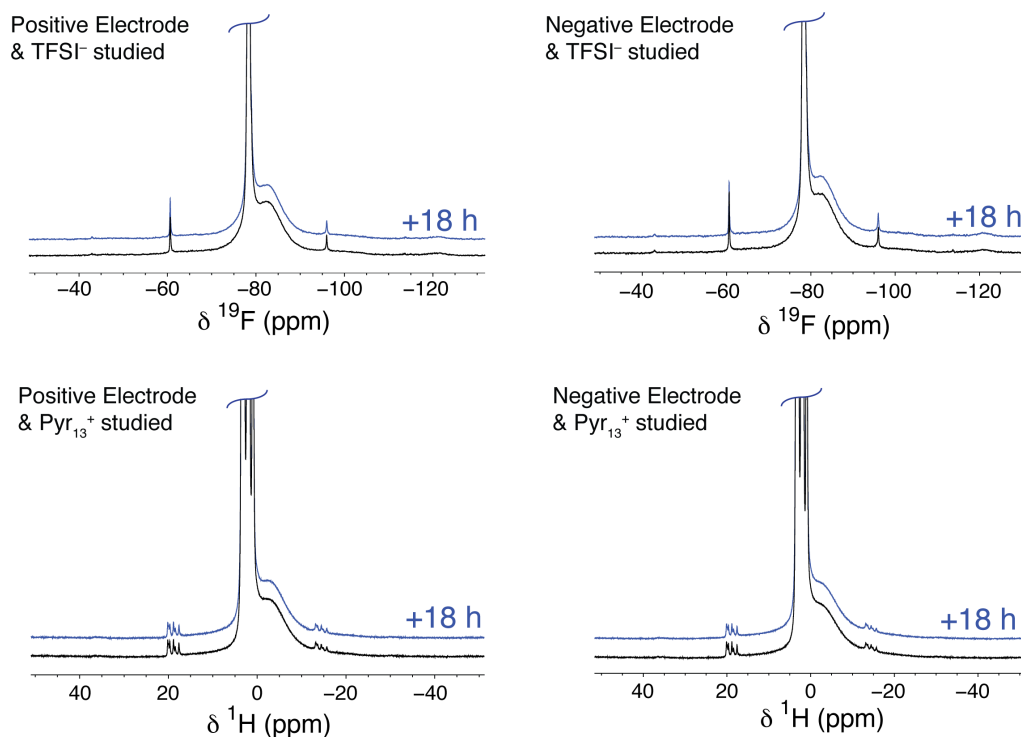


Figure S2 ^{19}F and ^1H NMR (7.1 T) spectra of electrodes extracted from a coin cell comprising YP50F carbon and $\text{Pyr}_{13}\text{TFSI}$ ionic liquid charged to a cell voltage of 1 V. Spectra are shown shortly after samples were packed (black) and ~ 18 hours after sample packing (blue).

To see if *ex situ* spectra showed any time dependence we recorded spectra after samples were allowed to rest for ~ 18 hours. Spectra are shown for a cell voltage of 1 V in Figure S2, with the spectrum acquired within one hour of sample packing compared to the spectrum after resting for ~ 18 hours. Resting was not observed to have any effect on the intensity or chemical shifts of the in-pore resonances, suggesting that both the charge state of the carbon and the populations of anions and cations in the pores are not changing on this timescale.

S3. Spectral deconvolutions of *ex situ* NMR data

Spectra were deconvoluted using the SOLA package in Topspin software. One peak was used to fit each ex-pore resonance, and a single peak was used to fit the in-pore resonances, even with this comprised multiple overlapping resonances in the ^1H NMR spectra. Representative deconvolutions of *ex situ* NMR spectra are shown in Figure S3.

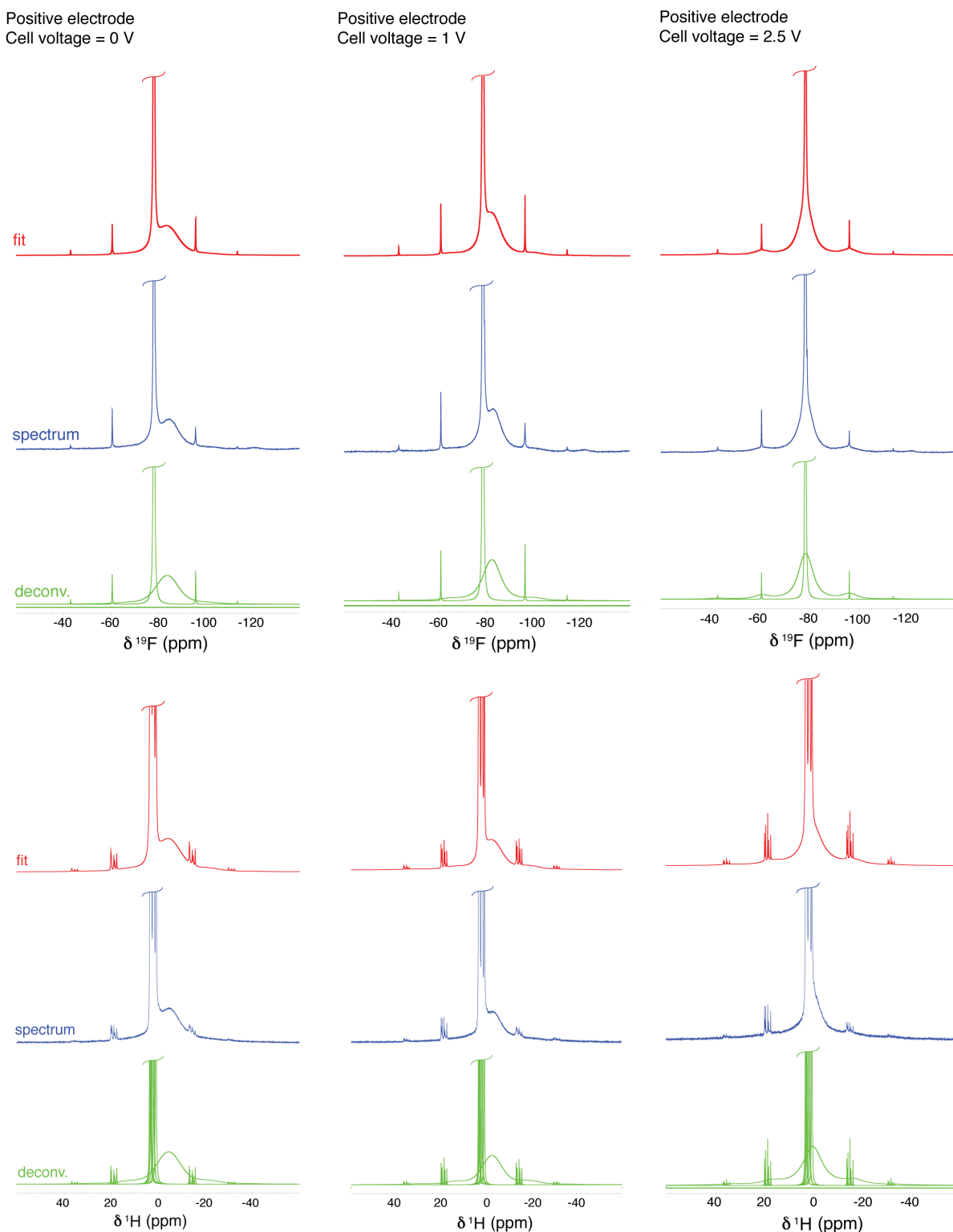


Figure S3 Representative spectral deconvolutions of *ex situ* NMR spectra.

S4. Variation of anisotropy upon charging

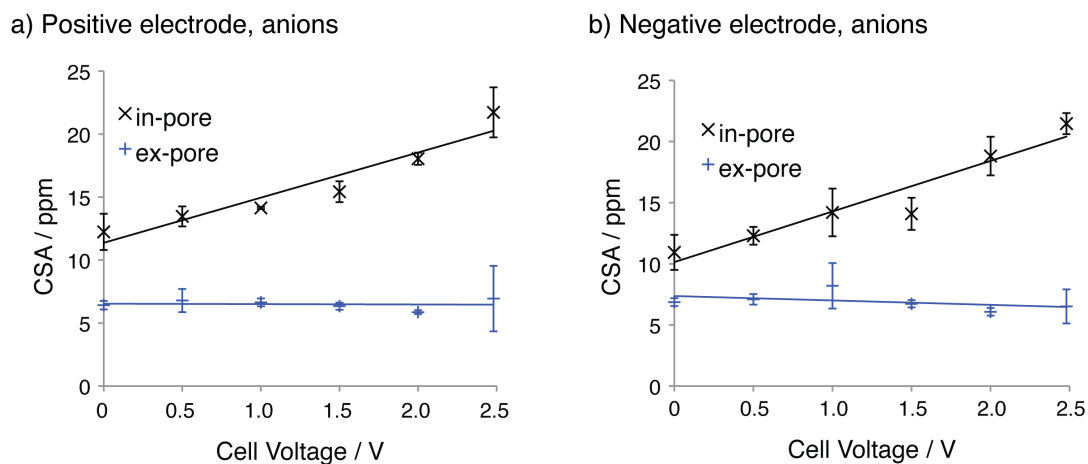


Figure S4 Variations of the chemical shift anisotropy obtained from fitting of ^{19}F *ex situ* NMR spectra.

Upon charging we observed an increase in the size of the in-pore spinning sidebands. This is quantified in Figure S4 where fitted chemical shift anisotropies (CSAs) are plotted against cell voltage. While the ex-pore environment shows no significant changes with voltage, the CSA of the in-pore environment increases in both electrodes. This suggests that charging reduces the mobility of in-pore anions in both electrodes.

S5. Variation of ^{19}F chemical shift for TFSI anions as a function of temperature

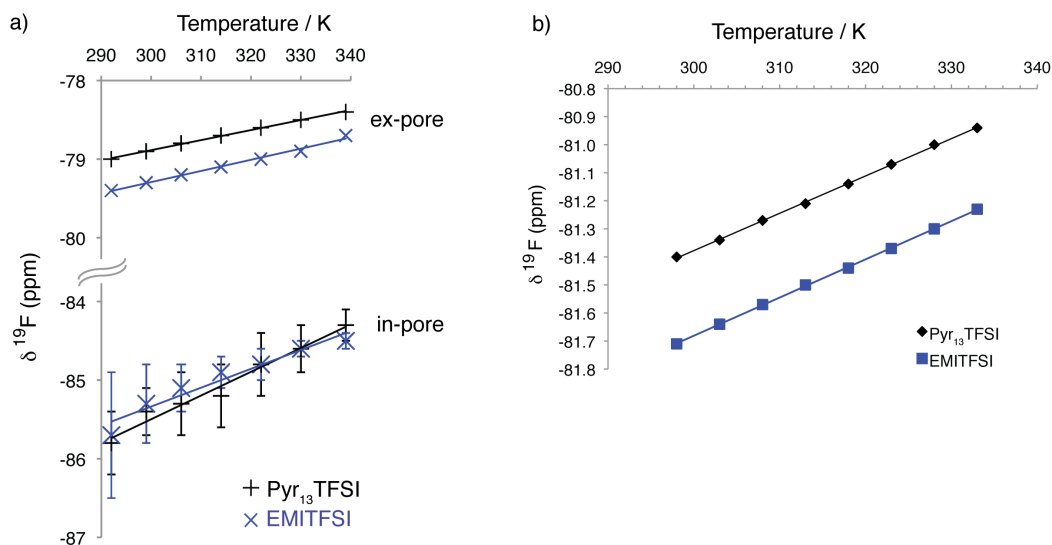


Figure S5 ^{19}F chemical shifts (9.4 T) as a function of temperature. (a) Shifts are shown for YP50F samples soaked with $\text{Pyr}_{13}\text{TFSI}$ and EMITFSI, and (b) for neat ionic liquids.

It was noted that ^{19}F chemical shifts showed some small temperature dependence in the main text. Measured chemical shift changes at 9.4 T are plotted in Figure S5a. As the temperature is increased, the chemical shifts increase (become less negative) in an apparently linear fashion for in- and ex-pore peaks for both $\text{Pyr}_{13}\text{TFSI}$ and EMITFSI ionic liquids. The increase of the ex-pore chemical shift with temperature is $12.5 \times 10^{-3} \text{ ppm}\cdot\text{K}^{-1}$ for $\text{Pyr}_{13}\text{TFSI}$ and $13.1 \times 10^{-3} \text{ ppm}\cdot\text{K}^{-1}$ for EMITFSI. These values are in good agreement with the shift variations observed for neat ionic liquid samples at the same magnetic field strength; 13.3×10^{-3} and $13.6 \times 10^{-3} \text{ ppm}\cdot\text{K}^{-1}$ for $\text{Pyr}_{13}\text{TFSI}$ and EMITFSI, respectively, shown in Figure S5b. For the in-pore resonances, slightly larger chemical shift variations of 30.1×10^{-3} and $24.0 \times 10^{-3} \text{ ppm}\cdot\text{K}^{-1}$ were measured for $\text{Pyr}_{13}\text{TFSI}$ and EMITFSI, respectively (Figure S5a). The observation of a stronger temperature dependence of the chemical shift for the in-pore resonance compared to the ex-pore suggests that the anion-carbon interactions show some temperature dependence. This may arise from a combination of several effects. First we note that at higher temperature the more confined adsorption sites may be less populated on entropic grounds. Second, exchange of the anions in and out of carbon pores, (i.e. exchange between the in- and ex-pore environments) will be faster at higher temperature. Both of these effects will tend to lengthen the average carbon-ion distances, thereby reducing the magnitude of the ring current shifts.

S6. Variable temperature ^1H NMR spectra of YP50F soaked with ionic liquid

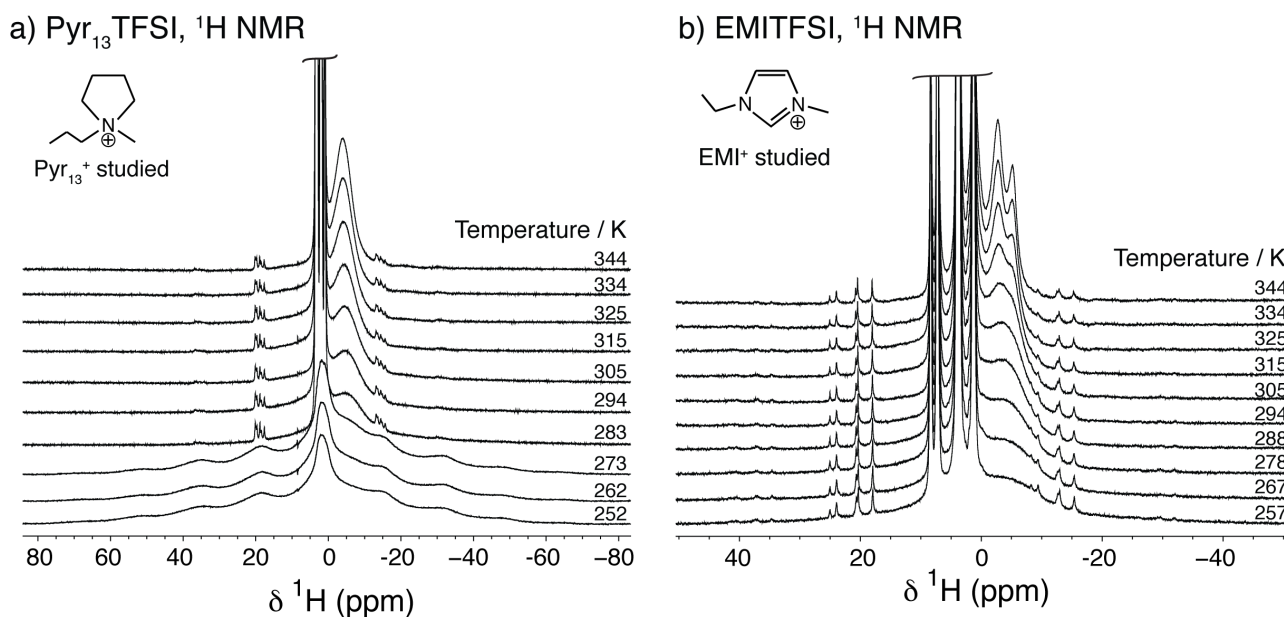


Figure S6 ^1H MAS NMR (7.1 T) spectra of YP50F samples soaked with a) Pyr_{13}^+ TFSI and b) EMITFSI ionic liquid. Spectra are recorded at a series of temperatures indicated in the figure.

^1H MAS NMR spectra of YP50F samples soaked with Pyr_{13}^+ TFSI and EMITFSI ionic liquids are shown in Figure S6. For both ionic liquids, motional narrowing effects are seen for the in-pore resonances as the temperature is increased. As discussed in the main text, increases in temperature result in faster diffusion of cations between different adsorption sites in the carbon micropores, narrowing the in-pore resonances. For EMITFSI, the in-pore resonances arising from the different chemical environments in each cation (the various CH, CH_2 and CH_3 groups) begin to become resolvable at the highest temperatures studied. Below 273 K, for the sample with Pyr_{13}^+ TFSI, the ex-pore resonance becomes considerably broader and the spinning sideband manifold shows increases in intensity and width. As discussed in the main text this is due to freezing of the ex-pore ionic liquid.

S7. Multisite model for exchange

A program was written in Matlab software to probe the timescale of the exchange processes described in the main text. In the model a number of different resonance frequencies are first defined (Figure S7a), which are intended to represent the range of possible frequencies that may be experienced by ions inside the porous carbon structure. While it is difficult to know the exact form of this distribution, we can estimate its width of the basis of NICS calculations on model carbon fragments.¹ Such calculations suggest that values can vary from large negative values of ~ -16 ppm inside carbon slit pores, to small positive values of $\sim +2$ ppm at the edge of planar carbon fragments,^{1,2} giving a range of possible shifts for adsorbed ions on the order of 20 ppm. As such, in the first instance we studied a uniform distribution of frequencies spanning 20 ppm (Figure S7a).

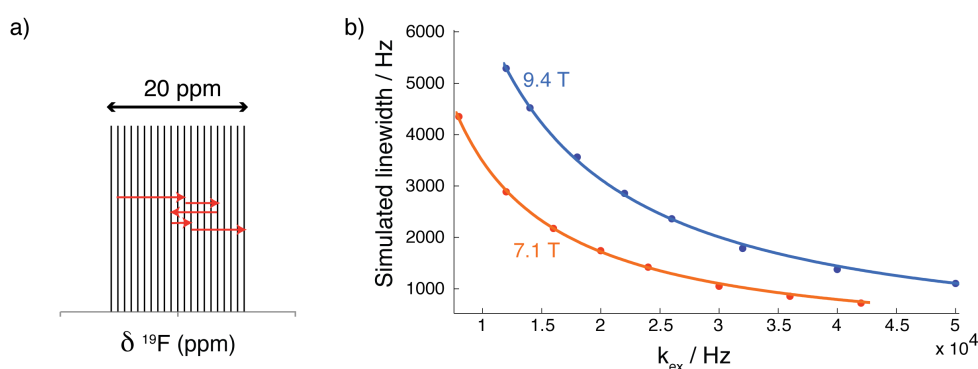


Figure S7 Distribution of chemical shift sites studied in the multi-site exchange model (a). The red arrows show the first five steps of one possible trajectory. Simulated lineshapes are shown in (b) for a range of different exchange rates and at two different magnetic field strengths. Stretched exponential fits of the simulated data are also shown.

In the simulations, the trajectories of different spins are computed as their resonance frequencies hop between the different possible values at an exchange rate, k_{ex} . Each time a frequency hop occurs, the new frequency of the spin is chosen at random from the possible values, i.e. we do not attempt to model the spatial arrangement of sites. The signals arising from an ensemble of 60 000 spins are summed and the resulting free induction decay is Fourier transformed to give the simulated NMR spectrum. A number of simulations were run with different k_{ex} values to study the effect of chemical exchange on the spectral lineshape. Simulated linewidths (full linewidth at half maximum peak intensity) are shown in Figure S7b for simulations carried out at two different magnetic field strengths. We found the simulated data could be well fit using stretched exponential functions.

The fitted stretched exponential functions were then used to extract k_{ex} values from the experimental linewidth data for in-pore anions. The natural logarithms of the extracted exchange rates are shown in Figure S8a. In principle, exchange rates extracted from spectra at the two different field strengths should be identical. For EMITFSI, this is the case within error, and for Pyr₁₃TFSI the agreement is also reasonable, giving us confidence in our approach. Exchange rates are well fit by straight lines,

consistent with a thermally activated Arrhenius-type exchange process. From the gradients of the plots in Figure S8a we obtain activation energies of 13 and 10 kJ·mol⁻¹ for in-pore motion of TFSI⁻ in EMITFSI and Pyr₁₃TFSI, respectively. While the energy barrier for motion of TFSI⁻ is slightly larger for EMITFSI, the timescale of exchange is faster for TFSI in EMITFSI than Pyr₁₃TFSI across the studied temperature range (Figure S8b). This is because the Arrhenius pre-factor, which may be thought of as the hopping attempt rate, is larger for EMITFSI (3.8×10^6 s⁻¹) than Pyr₁₃TFSI (1.0×10^6 s⁻¹). Hopping rates vary on the order of ~ 20 to 130μ s depending on the temperature and the ionic liquid studied. For example, at ambient temperature (294 K) the timescales for in-pore TFSI motion are 72 and 56 μ s for Pyr₁₃TFSI and EMITFSI, respectively. Motion is sped up at higher temperatures, with the respective timescales decreasing to 33 and 22 μ s.

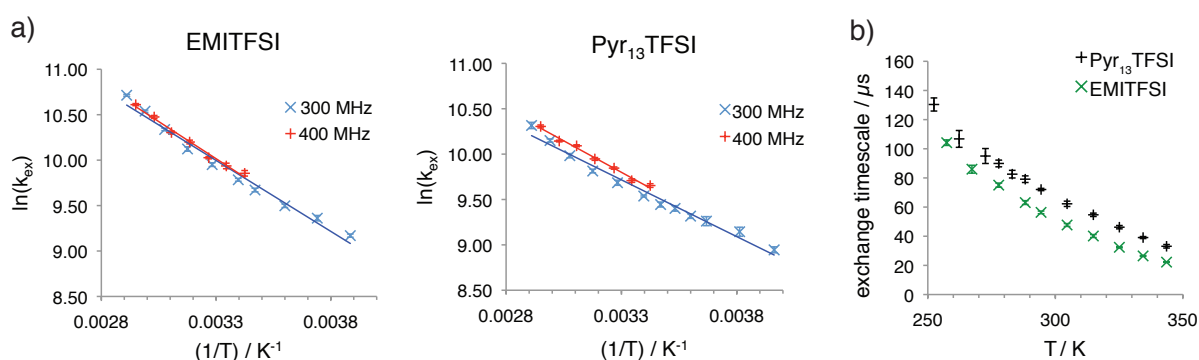


Figure S8 Natural logarithms of extracted exchange rates are plotted against inverse temperature in (a). In (b), exchange timescales (which are the inverse of the extracted exchange rates) are plotted against temperature.

It is interesting to explore the length scale associated with this exchange process. Assuming that the self-diffusion coefficient, D , for TFSI in neat Pyr₁₃TFSI at 292 K remains unchanged from that measured for free ionic liquid at $0.13 \times 10^{-10} \text{ m}^2 \cdot \text{s}^{-1}$,³ and considering a diffusion time, t , of 72 μ s (the simulated timescale for exchange for Pyr₁₃TFSI at 292 K above) this yields a diffusion distance of $(6Dt)^{0.5} = 75 \text{ nm}$ for the TFSI anions. This relatively large value of $0.075 \mu\text{m}$ may be compared to the typical carbon primary particle sizes that are on the order of 1 - 10 μm . In reality the diffusion value may be greatly reduced inside the tortuous network of the carbon micropores. For example, a two orders of magnitude reduction in the self-diffusion coefficient would reduce the estimated diffusion distance to 7.5 nm, *i.e.*, approaching the same order of magnitude of the size of the carbon fragments studied in the NICS calculations.

Finally, we note that the results obtained from the multi-site exchange simulation depend on the initial choice of the distribution of resonance frequencies. We explored other chemical shift distributions with different widths and profiles (e.g. Gaussian) and found that while the exact values of the extracted exchange rates and activation energies depend on the model used, the orders of magnitude of the exchange rates and activation barriers remain unchanged. We further note that the

lack of treatment of the complex spatial arrangement of adsorption sites in the carbon micropores will have a large effect on the results obtained in the simulation.⁴ In future work, more realistic simulations of chemical exchange, which take into account the connectivity of different sites in the heterogeneous carbon pore structure will provide more detailed insight into the exchange process observed here.

S8. Spectra for YP50F soaked with EMITFSI/dACN

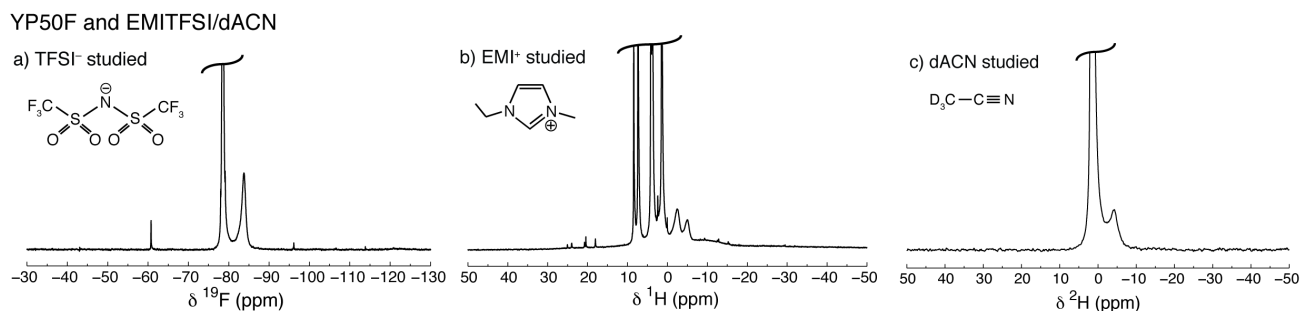


Figure S9 MAS NMR (7.1 T) spectra of YP50F films soaked with EMITFSI/dACN. a) ¹⁹F, b) ¹H and c) ²H spectrum.

MAS NMR spectra are shown in Figure S9 for YP50F samples soaked with EMITFSI/dACN. The concentration of the electrolyte is ~1.8 M. ¹⁹F, ¹H and ²H NMR experiments allow the study of the anions, cations and solvent respectively. Spectra of the anions and cations exhibit narrow in-pore resonances, compared to the spectra of analogous samples prepared using neat ionic liquid (see Figure 1 in the main text). This shows, as with Pyr₁₃TFSI, that the addition of acetonitrile solvent greatly increases the mobility of ions in the carbon micropores.

References

- (1) Forse, A. C.; Griffin, J. M.; Presser, V.; Gogotsi, Y.; Grey, C. P. *J. Phys. Chem. C* **2014**, *118*, 7508.
- (2) Xu, Y.; Watermann, T.; Limbach, H.-H.; Gutmann, T.; Sebastiani, D.; Buntkowsky, G. *Phys. Chem. Chem. Phys.* **2014**, *16*, 9327.
- (3) Hayamizu, K.; Tsuzuki, S.; Seki, S.; Fujii, K.; Suenaga, M.; Umebayashi, Y. *J. Chem. Phys.* **2010**, *133*, 194505.
- (4) Merlet, C.; Forse, A. C.; Griffin, J. M.; Frenkel, D.; Grey, C. P. *J. Chem. Phys.* **2015**, *142*, 094701.